JOTCS A
Journal of the Turkish Chemical Society
Section: A
Chemistry
TURKISH CHEMICAL SOCIETY

Synthesis and Photodegradation of Bi_2O_3 and Pb-Bi_2O_3 Nanoparticles and Their Kinetic Study

Farzana HAIDER*, Zakia GUL, Kafeel AHMAD KHAN

Department of Chemistry, Bacha Khan University, Charsadda, Pakistan

Abstract: The green synthesis method synthesized the bismuth oxide and lead-doped bismuth oxide nanoparticles using Ferula Asafoetida leaves extract. The lead-doped bismuth oxide showed greater degradation efficiency than undoped bismuth oxide. This greater efficiency was due to decreases in the band gap energy between the valence band and the conduction band of the metal oxide and reduced the chances of electron-hole pair recombination with the metal oxide catalyst. The synthesized nanoparticles were characterized by TGA, SEM, FT-IR, EDX, XRD, and UV- visible Spectrometer. XRD diffraction of Bi_2O_3 nanoparticles reflected a strong and sharp peak at 32.8° shows that Bi_2O_3 nanoparticles are in crystalline phase. The crystallite size of Bi_2O_3 nanoparticles is 13.433 nm, and Pb-doped Bi_2O_3 is 9.6 nm, calculated from the Debye-Scherrer equation. The synthesized Bi_2O_3 nanoparticles are round in shape with average size of ~ 90-100 nm While Pb doped Bi_2O_3 is ~ 75 f- 100 nm. The EDX spectra showed no additional peak for any impurities. The degradation rate of Malachite Green dye (MG) increased with the increase in contact time and temperature, while it decreased with increasing dye initial concentration and pH. Initially, the degradation efficiency of the bismuth oxide catalyst is increased with increasing catalyst amount, but after a certain amount of catalyst, it started decreasing as the catalyst amount was further increased. The irradiation time on photodegradation is deliberate, keeping other parameters steady at catalyst quantity 0.01 g at specific reaction conditions. Moreover, the dye showed an increase in degradation at 50 °C. The utmost degradation of 92% was observed for lead-doped bismuth oxide (Bi_2O_3) and 76% for undoped bismuth oxide (Bi_2O_3).

Keywords: Bi_2O_3 nanoparticles, Debye-Scherrer equation, dye degradation.

Submitted: August 18, 2022. **Accepted:** July 25, 2023.

Cite this: Haider F, Gul Z, Ahmad Khan K. JOTCSA. Synthesis and Photodegradation of Bi_2O_3 and Pb-Bi_2O_3 Nanoparticles and Their Kinetic Study. 2023; 10(4): 985-1000.

DOI: https://doi.org/10.18596/jotcsa.1164065.

Corresponding author. E-mail: unsty36@gmail.com.

1. INTRODUCTION

Nanotechnology has grown to be the most dynamic area of research in various fields of science, having an objective to determine the recompenses of the nano world for the betterment of society (1). Scientists use fine powders for various purposes, such as manufacturing, calculating, and characterization. Practical applications of nanotechnology are increasing with increasing demand for people. Scientists may also use nanotechnology in cosmetics (2), catalysis (3), medicines (4), and biosensing (5). Nanotechnology has a vital role in chemistry, fabric science, engineering, and physics (6).

Metallic nanoparticles are more significant than metal factors in the bulk state (7). Many nanoparticles have been manufactured from time to time. These fine powders were used in various applications such as terminals of batteries, catalyzers, and components of diesel (8). Bismuth oxide nanoparticles can be used in antibiotic-resistant pathogens on the atomic, thermal, and land physical properties. Bismuth oxide is used in numerous industries, such as optical electronics (9),

solid oxide fuels (10), and cell optical coating (11). It is widely used in applications such as gas sensors (12), optical technology (13), and microelectronics (14).

The plastic, textile, and pharmaceutical industries mainly add pollutants to the environment. These pollutants destroy or reduce the growth and production of local flora and fauna (15). Dyes released by these industries mainly cause water pollution, which reduces the penetration of sun light to water as sunlight is essential for both aquatic and land, so due to the unavailability of light, the plants are unable to synthesize their food. Dyes have diverse distinctiveness and affinities; for example, methylene blue (MB), congo red dye (CR), methyl orange (MO) dye, malachite green dye (MG), and 4-nitrophenol (4-NP) are natural dyes and pollutants. These dyes have complicated molecular structures and are non-biodegradable (16). The elimination of this pollutant from surroundings is of primary importance. Mostly NPs can be unique and best for removing such harmful substances (17).

The malachite green dye is water soluble cationic dye, green in color and crystalline powder in texture. To reduce water pollution, converting these dyes into non-hazardous forms is essential before they are released into water (18). Textile, pharmaceuticals, and leather industries use Nitro phenol (pollutant) for coloring and chemical synthesis, which pollutes the ecosystem. Nitro phenol and other chemicals move down the soil and contaminate the water. This contaminated water may cause mutation and cancer in living organisms. These cancer-causing pollutants are non-biodegradable by routine methods (19, 20).

Nanoparticles produced from plants are safe because toxic chemicals are not used compared to chemicals and physical procedures used for NPS extraction. Plants offer herbal capping marketers for NPs synthesis (21). Silver nanoparticles use diminishes after the surfacing and common use of antibiotics like insecticides and pesticides, but silver nanoparticles in combination with antibiotics are more efficacious (22). Synthesis of silver nanoparticles is low cost in terms of temperature and pressure. It is also non-toxic owing to its industry utilization plant-based AgNPs have been given unique locations in all fields of technological know-how, mainly in medical drugs inclusive for the remedy of wounds, cuts, scratches, burn up, fungal illnesses and different pores skin associated illness (23) From plant *Trianthema decandra*, gold NPs had been prepared which help in coating objects. The scientist takes more interest in manufacturing Gold Nps because gold can bind with organic molecules easily but have a high-cost value (24). M. Mohammadlou et al. synthesized magnetic iron oxide (FeO_2) NPs from leaves of *Glycosmis Mauritania*. Magnetic iron oxide (FeO_2) NPs are used for various purposes. Synthesis from the plant is non-toxic than physical procedure and chemicals used for its synthesis (3). The research interest of our group is to synthesize nanoparticles using plants which is easily approachable, non-toxic, cheap, and safe. Scientists have used different plants, but *Ferula asafoetida* is not used until now, so the plant we are interested in is *Ferula asafoetida*.

2. EXPERIMENTAL SECTION

2.1. Collection of Sample

Ferula asafoetida is widely grown naturally in Abbot Abad (Pakistan). The plants were uprooted and Collected at their Mature Stage during March.

2.2. Reagents

The chemicals used for the synthesis of nanoparticles were $Bi(NO_3)_2$ and $Pb(NO_3)_3$. The synthesized nanoparticles degraded the organic dye Malachite green with the chemical formula ($C_{23}H_{25}N_2Cl$). All the chemicals used were of analytical Grade.

2.3. Instrumentation

The prepared solutions were thoroughly mixed using a magnetic stirrer (Misong Scientific c., lto Korea). The obtained precipitates were filtered with the help of Whatman filter paper No. 1 (Millipore Corp., Bedford. Mass). The precipitate was dried in an oven (precision, ±1℃, 0.6 kW). The fully dried precipitates were placed in a muffle furnace at 200 ± 5℃ (Neycraft ™ JFF 2000 Furnace) for a few minutes. The samples were placed in UV light box for photocatalytic reactions using an ultra-violet light source. In order to disperse the particles the sample was centrifuged using an ultracentrifugation machine (Daihan Labtech Co. Ltd., Korea). A double beam UV-visible spectrophotometer (UV-1800 240v, Shimadzu Corporation) was used for determination of concentration and wavelength of maximum absorption. For functional group analysis IR spectra were recorded using a spectrophotometer (Perkin Elmer FT-IR spectrometer model 95120) rotary flash evaporator. The surface morphology and elemental composition were confirmed by using FE-SEM (QUANTA FEG 450) and EDX, respectively. The XRD (Bruker-D8 Advanced X-ray diffraction) was used to find out the crystallinity of the synthesized powder.

2.4. Preparation of Leaves Extract

Fresh leaves of *Ferula Asafoetida* were washed with doubly distilled water and dried in the shade at room temperature (22-25 ℃). The dried leaves were then crushed using a commercial blender (TSK-949, west point Furnace). The aqueous solution of powder leaves (1 g/100 mL) was placed in the soxhlet apparatus for 3 hours in solvent for continuous solvent extraction. After that, the extract was filtered, and then the sample was concentrated under a vacuum in a rotary flash evaporator. The concentrated extract was air-dried, taken in an air-tight bottle, and stored for further use.

2.5. Synthesis of Bismuth Oxide Nanoparticles

2.5.1. Bismuth oxide Nanoparticles

Bismuth oxide nanoparticles were synthesized by using the green synthesis method. A solution of 0.5 M $Bi(NO_3)_2$ was prepared in 100 mL double distilled water, and then 5 mL *Ferula Asafoetida* extract was

added dropwise to the prepared solution. The solution was placed on a magnetic stirrer at a constant stirring of 1200 rpm for 10-15 minutes to homogenize. The particles were placed for 2-3 min in the preheated muffle furnace (200 ± 5℃) for combustion, producing bismuth oxide (Bi_2O_3) nanoparticles. In order to remove impurities, the sample was washed several times with double distilled water. Furthermore, the synthesized nanoparticles were calcinated for 2 hours to attain purity. Finally, the dried bismuth oxide nanoparticles were stored in an air-tight container for further use.

2.5.2. Pb-Doped bismuth Oxide Nanoparticles

To synthesize lead-doped bismuth oxide nanoparticles, 0.05M $Pb(NO_3)_3$ was added to 0.5M $Bi(NO_3)_2$ solution and 5 mL *Ferula asafoetida* extract. The solutions were placed on a magnetic stirrer at a constant stirring of 1200 rpm for 10-15 minutes to homogenize. The obtained particles were placed for 2-3 min in the preheated muffle furnace (200 ± 5℃) for combustion, resulting in lead-doped bismuth oxide nanoparticles. In order to remove impurities, the sample was washed several times with double distilled water. Furthermore, the synthesized nanoparticles were calcinated for 2 hours to attain purity. Finally, lead-doped bismuth oxide nanoparticles were obtained; the particles were stored in an air-tight container for further use.

3. RESULTS AND DISCUSSION

3.1. SEM of Bi_2O_3 and Pb-Bi_2O_3 Nanoparticles

The SEM analysis of Bi_2O_3 is shown in Fig. 1 (a). It is clear from the micrographs that synthesized Bi_2O_3 nanoparticles are in round aggregation form. The average size of the nanoparticles calculated from the AGI method of Bi_2O_3 is ~ 90-100 nm, while Pb-doped Bi_2O_3 is ~ 75- 100 nm. The surface morphology is clear in the micrograph, and the aggregate of nanoparticles is uniformly distributed. While from the surface morphology of Pb doped Bi_2O_3 Fig 1 (b) the lead is small, agglomerating on Bi_2O_3.

3.2. EDX analysis of Bi_2O_3 and Pb-Bi_2O_3

Figure 3.2 (a) and (b) display the elemental composition analysis of lead-doped Bi_2O_3, with both elements in oxide form. The mass ratios for Pb, Bi, and O were 23.55, 31.51, and 44.95, respectively, as shown in Figure 4.2(b). Meanwhile, the atomic ratios were 39.84 for Pb, 57.07 for Bi, and 3.09 for oxygen. The EDX spectra did not reveal any additional peaks, indicating the absence of impurities. In contrast, the undoped Bi_2O_3, illustrated in Figure 2 (a), had mass ratios of 13.55 for C, 16.55 for O, and 69.90 for Bi. Correspondingly, the atomic ratios were 45.19 for C, 41.42 for O, and 13.39 for Bi.

3.3. TGA of Bi_2O_3 and Pb-Bi_2O_3 Nanoparticles

The thermal stability of pure Bi_2O_3 nanoparticles and Bi_2O_3 nanoparticles doped by Pb were investigated by thermal gravimetric analysis in Figure 3. The thermograms were recorded in the nitrogen atmosphere by heating the samples from 25 to 600 ℃. The TGA of Bi_2O_3 nanoparticles was almost stable with a little weight loss over the given temperature range due to the moisture absorption and combined water. Overall weight loss of 2% is due to moisture in a temperature range of 300 to 400 ℃.

The TGA of doped Bi_2O_3 nanoparticles shows weight loss at three stages. The first stage of weight loss from 100 to 200 ℃ is attributed to the volatilization of water molecules from the nanoparticles. The second stage of weight loss from 300 to 400 ℃ is attributed to the inorganic compound Pb contains a small amount of PbO_2, which is thermally decomposed from PbO_2 to PbO. The third stage of weight loss from 500 to 600 ℃ shows excellent thermal stability of Pb nanoparticles (25). This shows the high thermal stability of doped Bi_2O_3 nanoparticles. The overall stability of Bi_2O_3 is higher than the doped Bi_2O_3 at 600 ℃. The total weight loss in pure Bi_2O_3 is less than that of doped Bi_2O_3 (26).

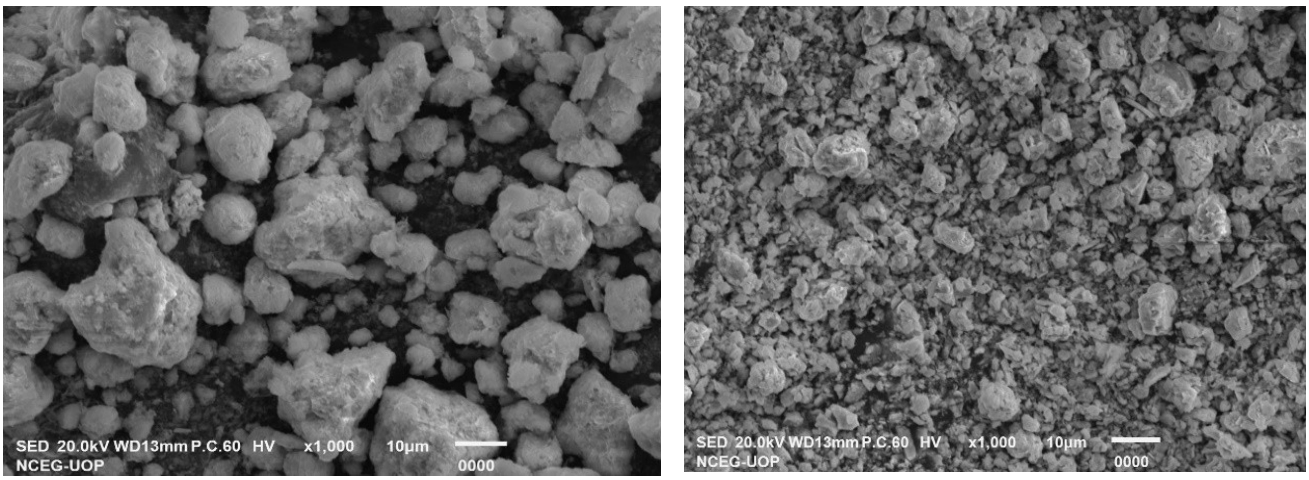

(a) (b)

Figure 1: SEM image for (a) Bi_2O_3 Nanoparticles (b) Pb-Bi_2O_3 nanoparticles.

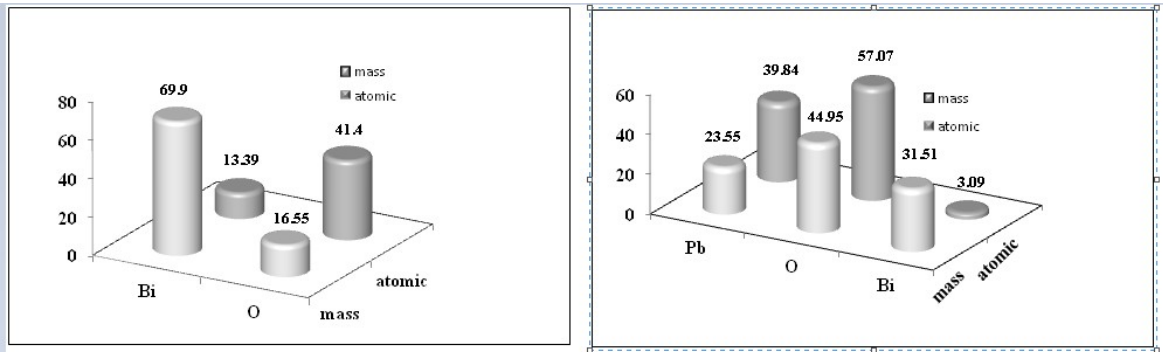

Figure 2: EDX analysis of (a) Bi_2O_3 (b) Pb-Bi_2O_3 Nanoparticles**.**

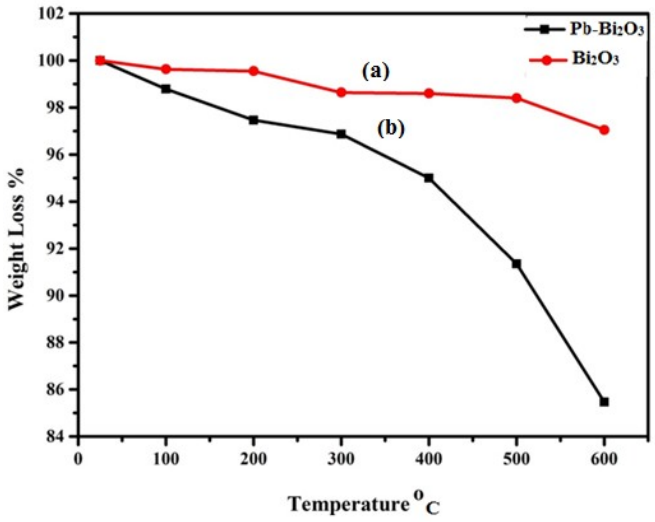

Figure 3: TGA of (a) Bi_2O_3 and (b) Pb-Bi_2O_3 nanoparticles.

3.4. FT-IR of Bi_2O_3 and Pb-Bi_2O_3

FT-IR spectra help study functional groups in a compound, their molecular interaction, and their molecular geometry. Figure 4 (a) shows the FTIR spectra of the calcined Bi_2O_3 and Pb-Bi_2O_3 nanoparticles. Generally, the band frequencies within 1000 cm^{-1} must be accredited to the bond stretching of metal oxides (27). The spectrum in Figure 4(a) at 3351.07 cm^{-1} is because of hydroxyl bond attraction in the water. The absorption spectrum obtained 1600- 1000 cm^{-1} is due to the occurrence of organic residue from the plant leaf extract. The peaks lower than 1000 cm^{-1} showed the presence of nanoparticles (28). Figure 4 (b) shows the absorption spectrum 675.49 cm^{-1} due to the stretching frequency of the Bi-O bond, and for Pb-Bi_2O_3 is 465.33 cm^{-1} because of Pb–O stretching (29). The result shows that Pb successfully merged in Bi_2O_3 crystal.

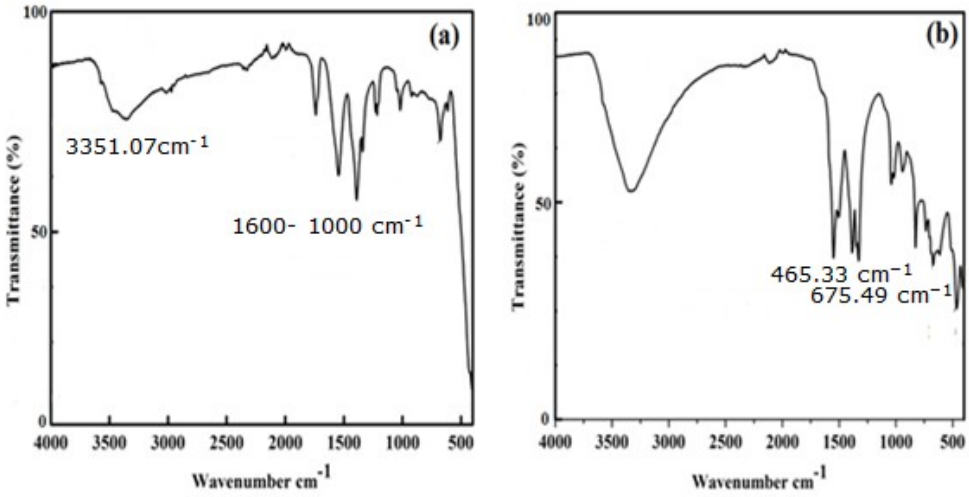

Figure 4: FTIR spectrum of (a) Bi_2O_3 and (b) Pb- Bi_2O_3 Nanoparticles.

3.5. XRD of Bi_2O_3 and Pb-Bi_2O_3 Nanoparticles

XRD is the most effective tool for describing the structure and nature of a material. An analytical technique mainly used to identify the crystalline nature of the material. In this technique, an X-ray is bombarded on the crystal. The crystalline properties and purity of the green synthesized Bi_2O_3 NPs were analyzed by X-ray diffraction data collected in the 2θ range. Fig. 5 (a) shows the XRD spectrum of Bi_2O_3. XRD diffraction of Bi_2O_3 nanoparticles gives a strong and sharp peak at 32.8˚, which confirms the crystalline nature of Bi_2O_3. The Bi_2O_3 nanoparticles exhibited peaks at 23.9˚, 29.2˚, 30.3˚, 32.0°, 47.09˚, 56.8˚, 42.3˚. Figure 5 (b) sharp peak at 2θ = 28.8°and 32.7˚ was observed for Pb- Bi_2O_3. JCPDS-card no -36-034 for Bi_2O_3 and pb-Bi_2O_3 JCPDS card no 3-0591. The Debye-Scherrer (Equation 1) was used to calculate the average crystallite size of Bi_2O_3 nanoparticles.

$$D=\frac{k\lambda}{\beta\cos\theta} \qquad \text{(Eq. 1)}$$

The average crystallite size is denoted by D, where k is the dimensionless shape factor with a value of 0.9 close to unity; it varies depending upon the crystallite's shape λ is the wavelength of the X-ray used, and β is the angle of diffraction at full width at half maximum. The crystallite size of Bi_2O_3 nanoparticles is 13.433 nm. The crystallite size of Pb-Bi_2O_3 nanoparticles is 9.6 nm Figure 5 (a) shows that X-ray diffraction peaks of Bi_2O_3 nanoparticles exhibited reflection peaks at 32.8˚ of glancing angle. The sharp crystalline peak shows that the nanoparticles are crystalline in structure (30).

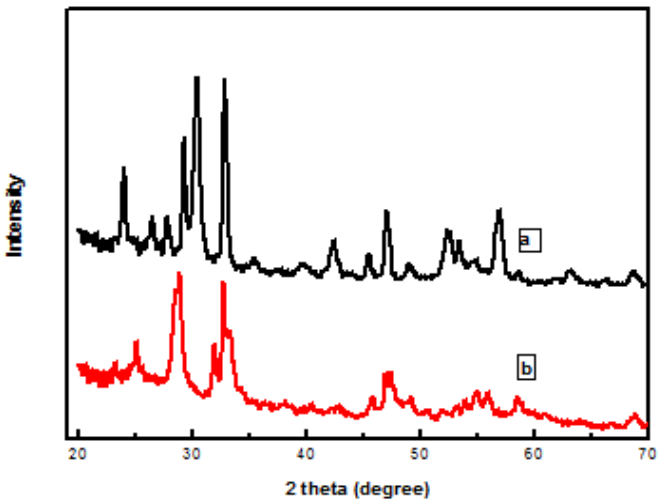

Figure 5: XRD patterns of (a) Bi_2O_3 (b) Pb-Bi_2O_3 Nanoparticles.

3.6. Photocatalytic Activity of Bismuth Oxide Nanoparticles

The photocatalytic activity of bismuth oxide and lead-doped bismuth oxide was studied under UV light to degrade malachite green dye. The effect of various parameters such as catalyst dose, irradiation time, initial dye concentration, pH, and temperature was observed.

3.7. Effect of Irradiation Time

UV light plays a primary role in the photodegradation of malachite green dye. The result showing irradiation time on photodegradation is deliberate, keeping other parameters steady at catalyst quantity 0.01 g, pH 4, time interval 120 minutes, and dye initial concentration 50 ppm, as shown in Figure 6(a). Irradiation time increases by increasing the degradation activity of bismuth oxide nanoparticles. This may be related to the amount of photo-generated electron-hole pair produced due to the sensitization of photocatalyst nanoparticles (31). Under UV light, dye degradation at different time phases is studied. Figure 6(a) depicts a lead-doped bismuth oxide that shows maximum degradation of 98%. The undoped bismuth oxide showed 91% degradation efficiency under a similar experimental condition, as shown in Figure 6(b).

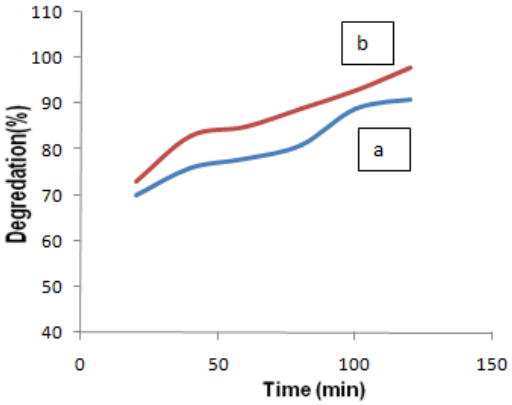

Figure 6a: Effect of irradiation time on photocatalytic degradation of MG dye by (a) lead-doped bismuth oxide (Bi_2O_3), (b) undoped bismuth oxide at catalyst amount of 0.01 g, pH 4, dye initial concentration of 50 ppm, irradiation time 120 minutes.

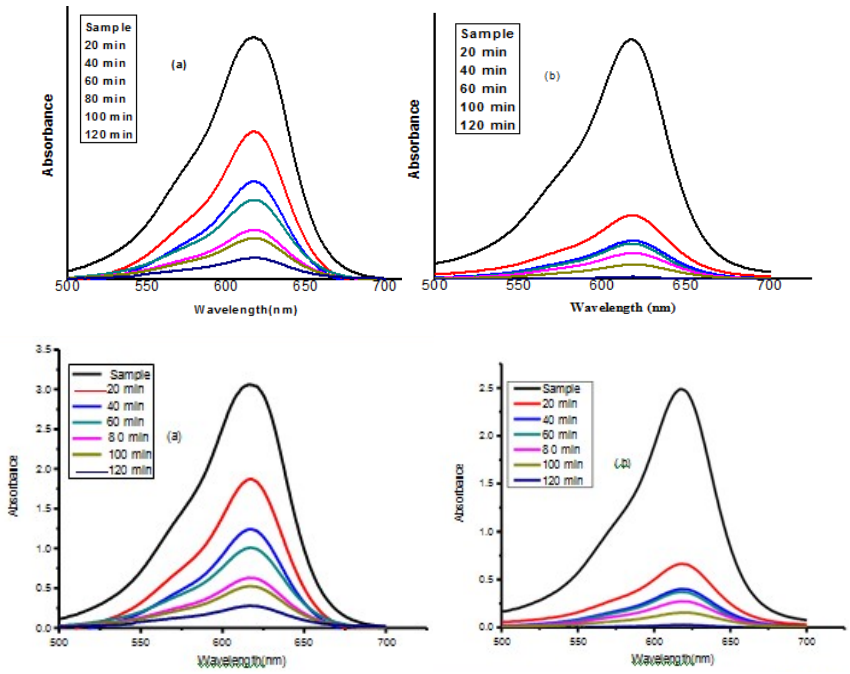

Figure 6b: Absorption spectra showing the effect of irradiation time on photocatalytic degradation of Malachite green dye (a) doped and (b) undoped bismuth oxide.

3.8. Effect of Dye Concentration

The effect of dye initial concentration on the photodegradation of dye is studied while keeping constant other parameters such as catalyst amount (0.01 g), pH (4), and time interval (120 minutes). It was studied that when the dye's initial concentration increases, then photodegradation decreases; it may be outstanding to the fact that light penetration to nanoparticles surface decreases when dye concentration is increased (9). More dye molecules will attach in active sites, extensively changing the photodegradation process. It was studied that at little concentration of 50 ppm maximum degradation of 98% for lead-doped bismuth oxide (Bi_2O_3), as shown in Figure 7(a), and 91% for undoped bismuth oxide (Bi_2O_3) was observed as depicted in Figure 7(b).

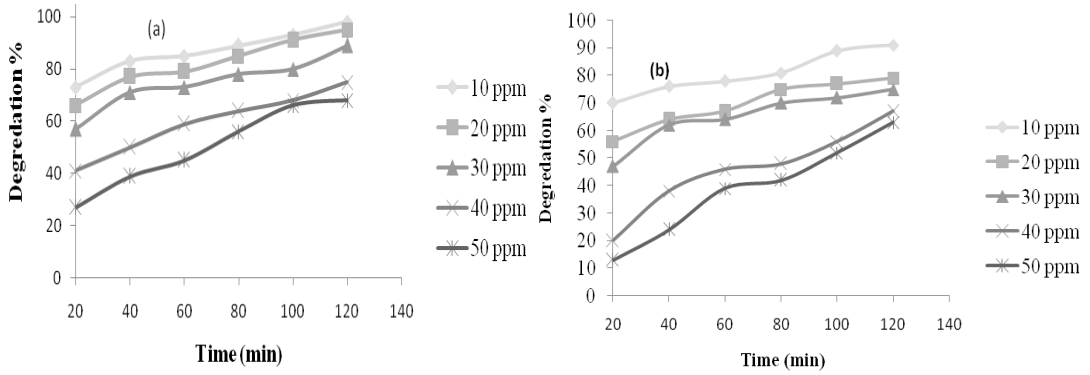

Figure 7: Effect of dye initial concentration on photocatalytic degradation of Malachite green dye by (a) lead-doped bismuth oxide (b) undoped bismuth oxide, at catalyst amount 0.01 g, initial dye pH 4.

3.9. Effect of Catalyst

The influence of varying catalyst amounts on the photodegradation of the dye was examined using different quantities of catalyst (10 mg, 15 mg, 20 mg, 25 mg, and 30 mg), with a constant radiation time of 120 minutes, an initial dye concentration of 50 ppm, and a pH level of 4. It was observed that the initial degradation rate increased with the addition of more catalysts but subsequently decreased. The reaction rate initially grew with the addition of more catalysts, reaching an optimal level, after which the nanoparticles began to act as a filter for the incident light, limiting the light intensity from reaching the semiconductor surface (10). The maximum degradation achieved was 82% for lead-doped catalyst, as shown in Figure 8(a), and 79% for undoped bismuth oxide nanoparticles, at an optimal catalyst amount of 20 mg, as illustrated in Figure 8(b).

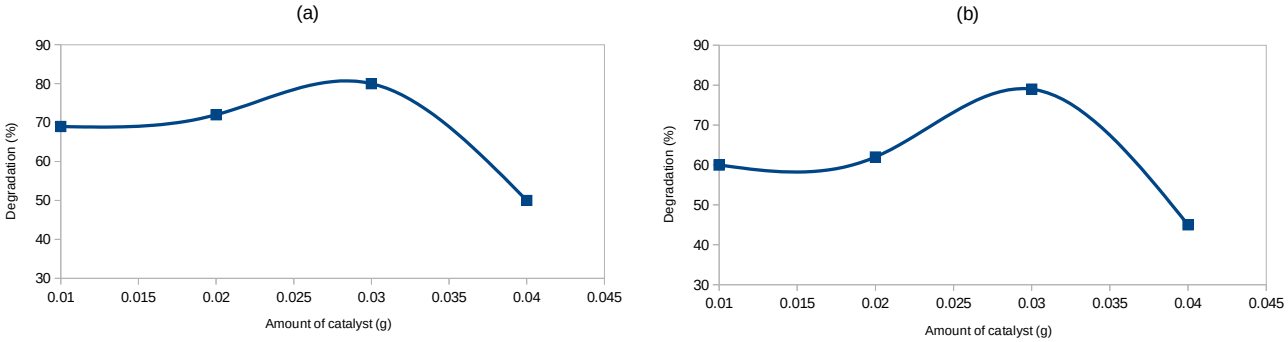

Figure 8: Effect of catalyst dose on photocatalytic degradation of MG dye by (a) lead-doped bismuth oxide, (b) undoped bismuth oxide, at catalyst amount 0.01 g, pH 4, and dye initial concentration 50 ppm and time interval 120 minutes.

3.10. Effect of pH

The effect of pH on the photodegradation of dye was studied at various pH (4, 5, 10, and 11) at a constant radiation time of 120 minutes with a dye concentration of 50 ppm initial and a catalyst quantity of 10 mg. It was observed that the rate of degradation increases as pH increases (32). The maximum degradation efficiencies of 79% for lead-doped bismuth oxide in Figure 9(a), while 75% for undoped bismuth oxide was obtained as shown in Figure 9(b).

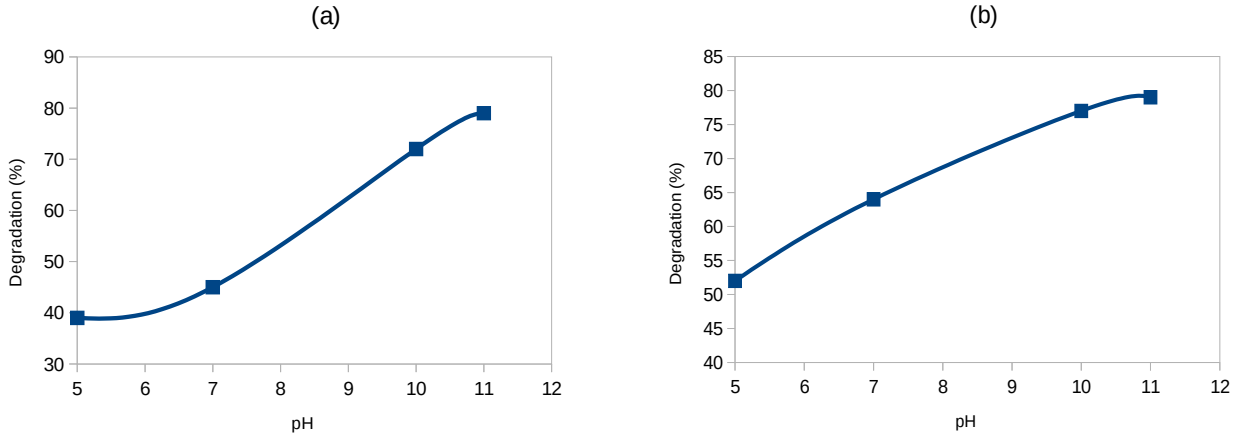

Figure 9(a, b): Effect of pH on the photocatalytic degradation of MG dye by (a) lead-doped bismuth oxide (Bi_2O_3) (b) undoped bismuth oxide, at Catalyst amount 0.01 g, dye initial concentration 50 ppm, and irradiation time 120 minutes.

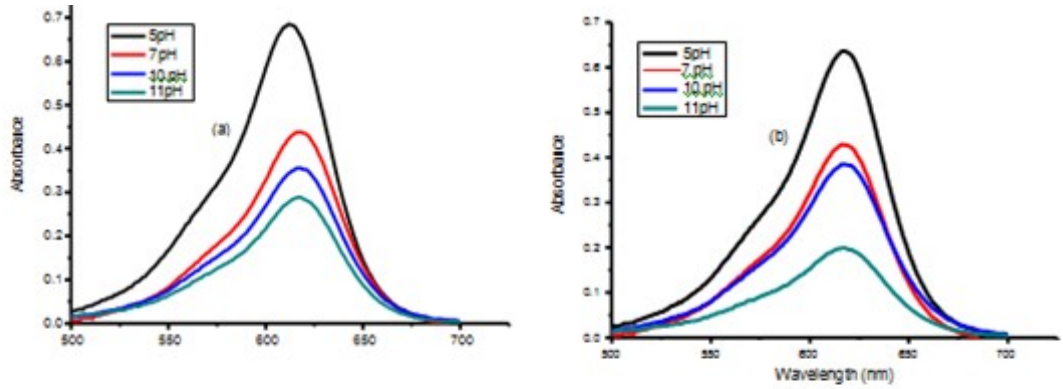

Figure 9c: Absorption spectra effect of pH on the photocatalytic degradation of malachite green dye (a) doped (b) undoped bismuth oxide (Bi_2O_3).

3.11. Effect of Temperature

In the photodegradation of dye, temperature plays a significant role. At different temperatures (30, 40, and 50 °C), the dye degradation was studied, keeping the other parameters steady, i.e., irradiation time 120 minutes, 50 ppm initial dye concentration, and catalyst amount of 10 mg. It was experimentally observed that with the temperature increase, dye degradation increased, and the utmost degradation of 92% for lead-doped bismuth oxide in Figure 10(a) and 76% for undoped bismuth oxide was achieved in Figure 10(b).

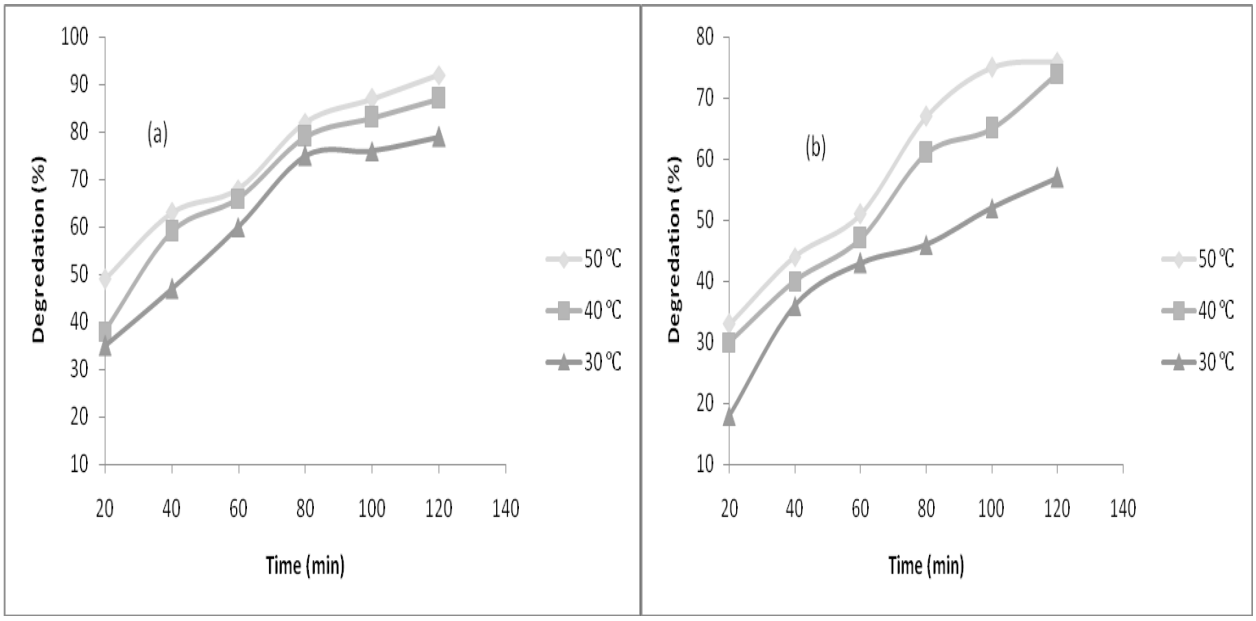

Figure 10(a, b): Effect of temperature on photocatalytic degradation of Malachite green dye by (a) lead-doped bismuth oxide (b) undoped bismuth oxide, catalyst amount 0.01 g, pH 4, time initial concentration 50 ppm and time interval 120 minutes.

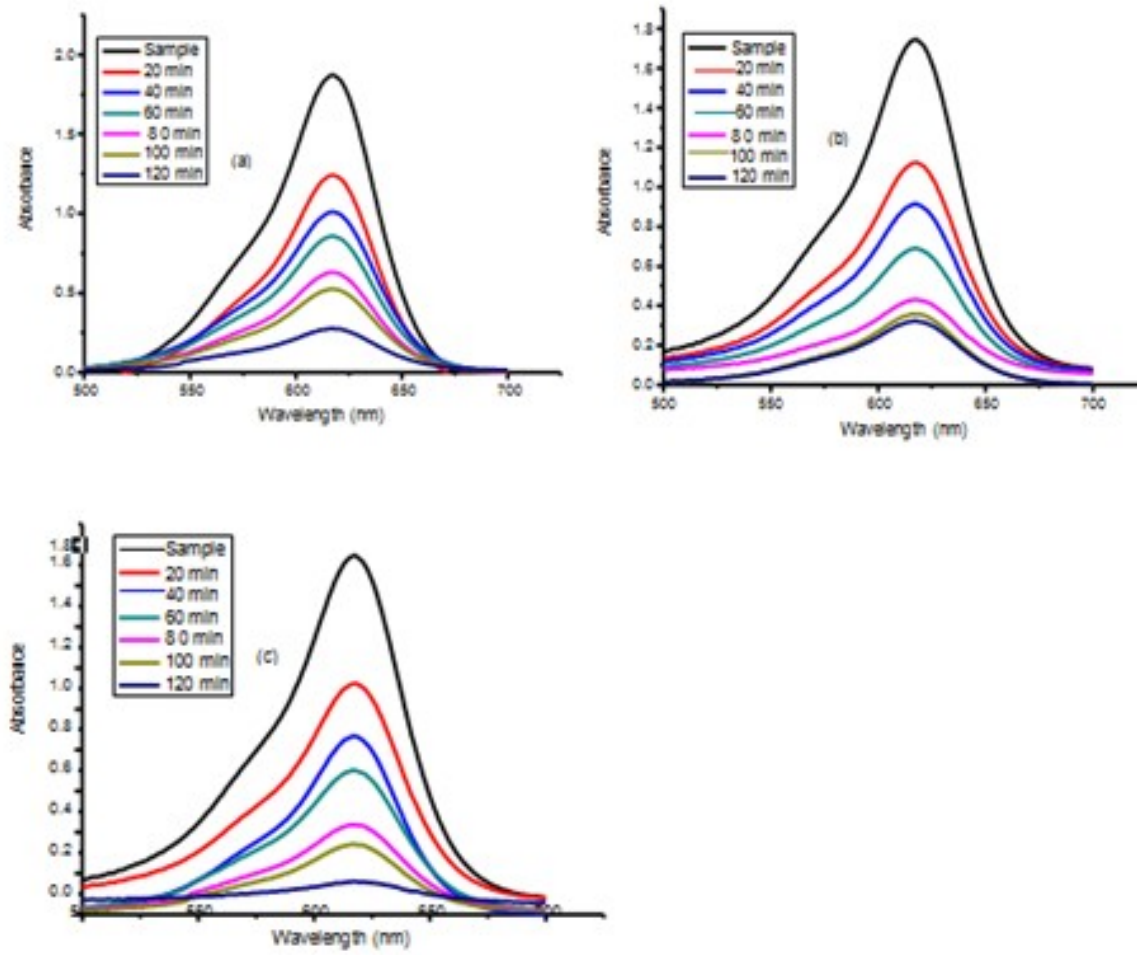

Figure 10c: Absorption spectra showing effect of immediate time at constant (60 ℃) on the photocatalytic degradation of MG dye (a) (b) (c) for lead-doped bismuth oxide.

3.12. Kinetic Study of Nanoparticles

The Kinetic study of degradation of MG at different temperatures (30 ºC, 40ºC, 50 º C) by using different concentrations (10 ppm, 20 ppm, 30 ppm, 40 ppm, 50 ppm) of doped Bi_2O_3 and undoped Bi_2O_3 as a catalyst. The k values linearization was used to calculate the temperature parameters of doped Bi_2O_3 and undoped Bi_2O_3. Table 1 presents the values of R^2, extracted from the linearization of the rate constants (k) by Bi_2O_3. With increasing the concentration of catalyst, the rate of degradation decreases. However, the same trend was observed for temperature parameters. The photodegradation of the samples was evaluated at a different temperature by applying the following equations (Eq. 2 and 3).

$$\frac{dc}{dt} = k_{App} \times C \qquad \text{(Eq. 2)}$$

where k_{App} is called the pseudo-first-order rate constant.

The integrated form of the above equation is

$$\ln\left(\frac{C_0}{C}\right) = k_{App} \times t \qquad \text{(Eq. 3)}$$

C_0 and C represent the initial and final concentration of MG dye, respectively.

Figure 11(a) and 11(b) show the kinetic study of MG dye. It can be observed that the rate of photocatalytic reaction is significantly affected by the catalyst dose. The k_{App} and their correlation coefficient values for undoped and Pb-doped Bi_2O_3 are given in Tables 1 and 2.

Table 1: Parameter of pseudo-first-order kinetics equation of different temperatures using Pb -Bi_2O_3.

Temp (ºC)	Equation	R^2	kA_{pp}
30	y = 0.0136x + 0.1619	R^2 = 0.9679	0.0136
40	y = 0.0186x + 0.186	R^2 = 0.954	0.0186
50	y = 0.018x + 0.1134	R^2 = 0.9778	0.018

Table 2: Parameter of pseudo first order kinetics equation of different temperatures using undoped Bi_2O_3.

Temp (ºC)	Equation	R^2	kA_{pp}
30	y = 0.0117x + 0.1335	R^2 = 0.9586	0.0117
40	y = 0.0098x + 0.1276	R^2 = 0.9824	0.0098
50	y = 0.006x + 0.1531	R^2 = 0.9558	0.006

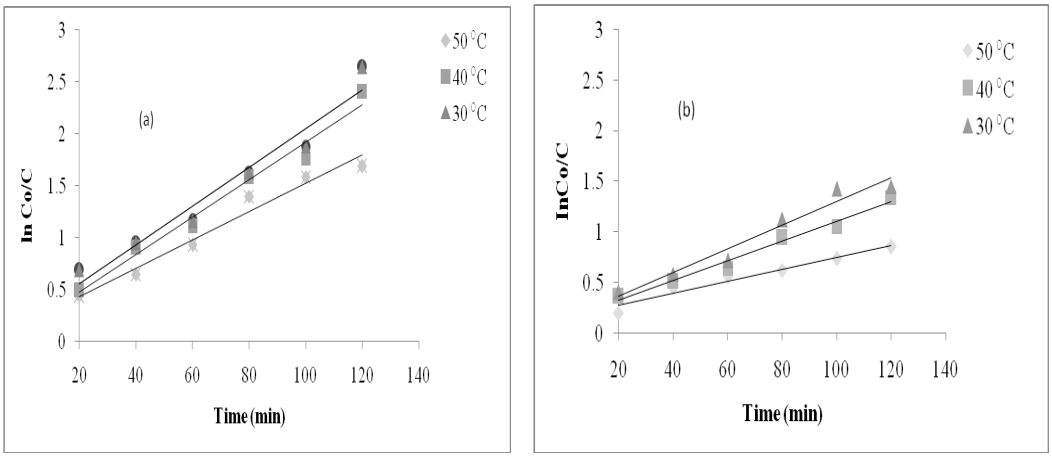

Figure 11: Showing the application of pseudo 1st orders kinetic to photodegradation of dye on (a) Pb -Bi_2O_3 (b) undoped Bi_2O_3 at different temperatures.

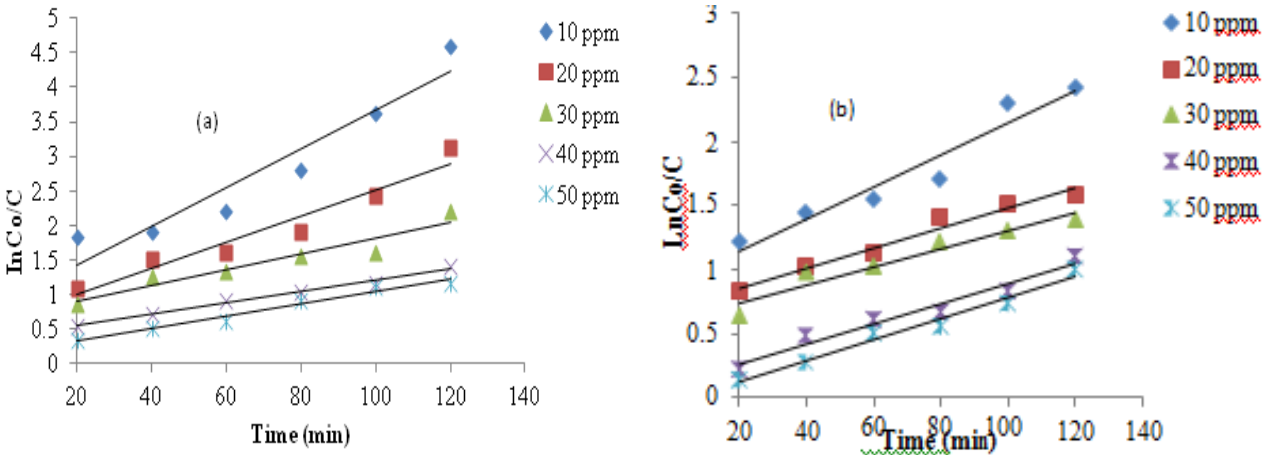

Figure 11c: Application of pseudo first order kinetic to photodegradation of dye on (a) Pb -Bi_2O_3 (b) undoped Bi_2O_3 at different concentrations.

Table 3: Parameter of first-order kinetics equation of different concentrations using undoped Bi_2O_3.

Conc. (mg/L)	Equation	R^2	kA_{pp}
10	y = 0.0125x + 0.897	R^2 = 0.9348	0.0125
20	y = 0.0078x + 0.6997	R^2 = 0.9656	0.0078
30	y = 0.007x + 0.6016	R^2 = 0.927	0.007
40	y = 0.0079x + 0.1069	R^2 = 0.9604	0.0079
50	y = 0.0082x - 0.0359	R^2 = 0.9753	0.0082

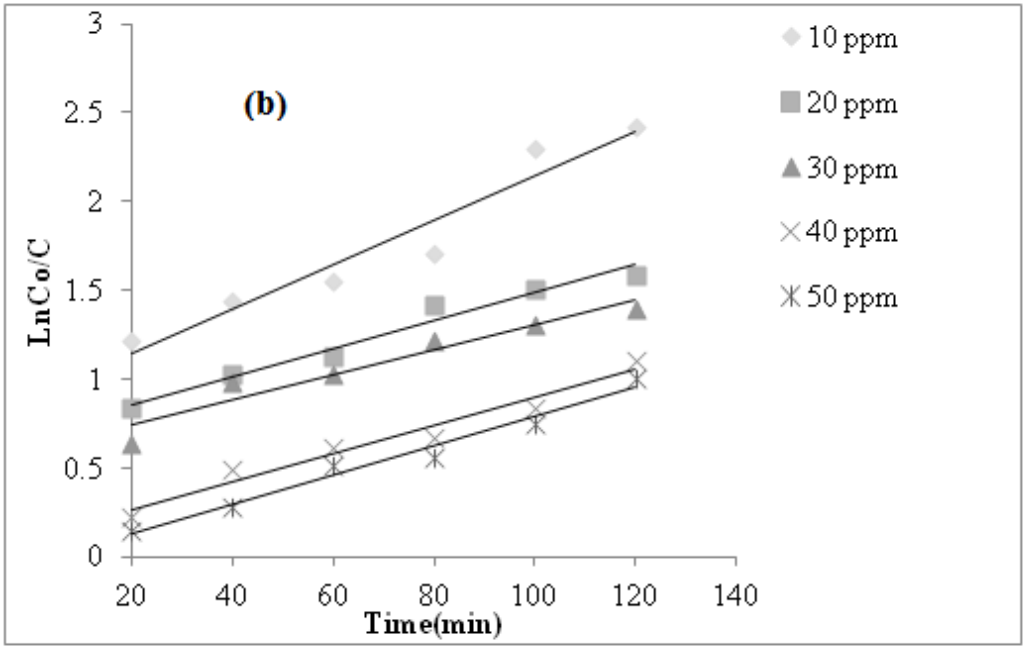

Figure 11(d): Application of pseudo first order kinetic to photodegradation of dye on Pb-Bi_2O_3 at different concentrations.

Table 4: Parameter of first-order kinetics equation of different concentrations using Pb-Bi_2O_3.

Conc.(mg/L)	Equation	R^2	kA_{pp}
10	y = 0.0279x + 0.8719	R^2 = 0.9141	0.0279
20	y = 0.019x + 0.6111	R^2 = 0.9405	0.019
30	y = 0.0115x + 0.6653	R^2 = 0.9027	0.0115
40	y = 0.0084x + 0.3716	R^2 = 0.9873	0.0084
50	y = 0.0089x + 0.1458	R^2 = 0.9723	0.0089

3.13. Arrhenius Equation

The effect of temperature was studied at 50 ppm dye concentration, irradiation time 120 min with catalyst amount 10 mg. A linear relation was found between lnk and 1/T with a negative slope for doped Bi_2O_3 and undoped Bi_2O_3 nanoparticles, as shown in Figure 12(a, b).

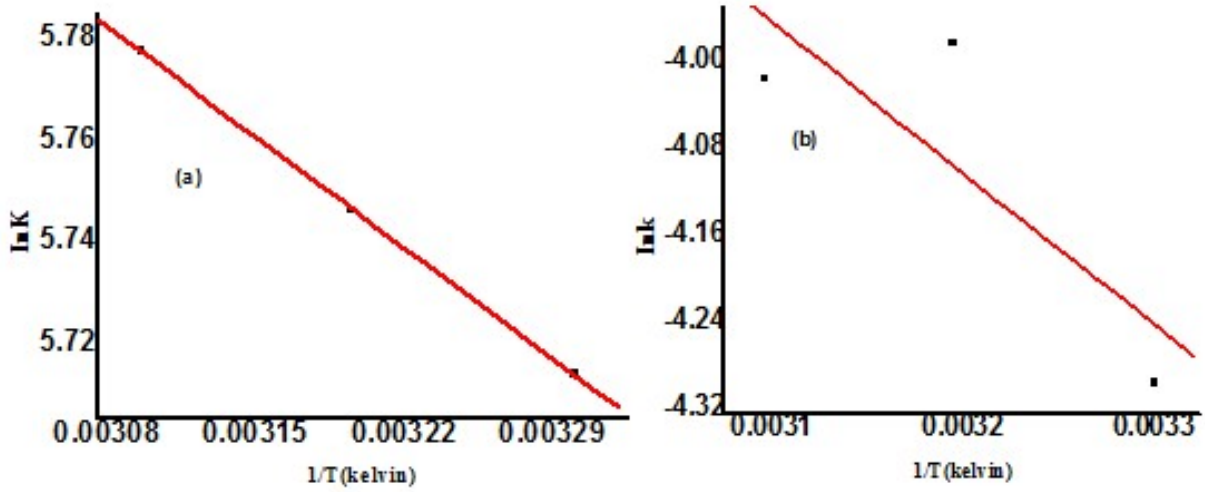

Figure 12: Arrhenius plot lnk vs. 1/T (a) doped (b) undoped Bi_2O_3.

4. CONCLUSION

Many processes have been used for water purification, but out of all these various processes employed, a major improvement of the photocatalytic activity was observed in the system using a combination of oxidant and photocatalyst irradiation under ultraviolet light. The concentration of both the oxidant and the photocatalyst greatly influenced the degradation rate. Also, the process was observed to be strongly pH dependent. Photodegradation could be an advocate approach for managing wastewater containing MG dye as a pollutant. The study found that the degradation process depends on various parameters like temperature, pH, dye concentration, amount of catalyst, and contact time; by changing any of the above parameters, the extent of degradation changed. The optimum conditions for degradation of Malachite Green dye by bismuth oxide catalyst were pH 4, catalyst amount 0.03 g dye initial concentration 50 ppm, contact time 120 minutes, and temperature 30 ℃. The techniques such as SEM, FTIR, XRD, and TGA analysis indicated satisfactory formation of NPs. The bismuth oxide nanoparticles have an average size of 90 nm, and lead-doped bismuth oxide is 75 nm, showed by SEM analysis. The FTIR spectrum shows the occurrence of alcoholic compounds and metal oxide in the *Ferula Asafoetida* leaves extract. However, the TGA of undoped Bi_2O_3 nanoparticles was almost stable with a little weight loss (2%). The total weight loss in pure Bi_2O_3 was less than the doped Bi_2O_3. XRD diffraction of Bi_2O_3 nanoparticles reflected a strong and sharp peak at 32.8˚, showing that Bi_2O_3 nanoparticles are in the crystalline phase. The crystallite size of Bi_2O_3 nanoparticles is 13.433 nm, and Pb-doped Bi_2O_3 is 9.6 nm, calculated from the Debye-Scherrer equation.

5. REFERENCES

1. Heera P, Shanmugam S. Nanoparticle characterization and application: an overview. Int J Curr Microbiol App Sci. 2015;4(8):379–86.

2. Hani Ramli R, Soon CF, Mohd Rus AZ. Characterisation of silver nanoparticles produced by three different methods based on Borohydride reducing agent. Sharif S, Abdullah MMAB, Abd Rahim SZ, Ghazali MF, Mat Saad N, Ramli MM, et al., editors. MATEC Web Conf. 2016;78:01032. Available from: <URL>.

3. Mohammadlou M, Maghsoudi H, Jafarizadeh-Malmiri H. A review on green silver nanoparticles based on plants: Synthesis, potential applications and eco-friendly approach. International Food Research Journal. 2016;23(2):446.

4. Miri A, Sadat Shakib E, Ebrahimi O, Sharifi-Rad J. Impacts of Nickel Nanoparticles on Grow Characteristics, Photosynthetic Pigment Content and Antioxidant Activity of Coriandrum sativum L. Orient J Chem. 2017 Jun 28;33(3):1297–303. Available from: <URL>.

5. Duman F, Ocsoy I, Kup FO. Chamomile flower extract-directed CuO nanoparticle formation for its antioxidant and DNA cleavage properties. Materials Science and Engineering: C. 2016 Mar;60:333–8. Available from: <URL>.

6. Geethalakshmi R, Sarada DVL. Characterization and antimicrobial activity of gold and silver nanoparticles synthesized using saponin isolated from Trianthema decandra L. Industrial Crops and Products. 2013 Nov;51:107–15. Available from: <URL>.

7. Firdhouse MJ, Lalitha P, Sripathi SK, others. Novel synthesis of silver nanoparticles using leaf ethanol extract of Pisonia grandis (R. Br). Der Pharma Chemica. 2012;4(6):2320–6.

8. Gangula A, Podila R, M R, Karanam L, Janardhana C, Rao AM. Catalytic Reduction of 4-Nitrophenol using Biogenic Gold and Silver Nanoparticles Derived from *Breynia rhamnoides*. Langmuir. 2011 Dec 20;27(24):15268–74. Available from: <URL>.

9. Raza W, Haque MM, Muneer M, Harada T, Matsumura M. Synthesis, characterization and photocatalytic performance of visible light induced bismuth oxide nanoparticle. Journal of Alloys and Compounds. 2015 Nov;648:641–50. Available from: <URL>.

10. Falagas ME, Fragoulis KN, Karydis I. A Comparative Study on the Cost of New Antibiotics and Drugs of Other Therapeutic Categories. Baune B, editor. PLoS ONE. 2006 Dec 20;1(1):e11. Available from: <URL>.

11. Camilleri J. Color Stability of White Mineral Trioxide Aggregate in Contact with Hypochlorite Solution. Journal of Endodontics. 2014 Mar;40(3):436–40. Available from: <URL>.

12. Marchaim D, Lemanek L, Bheemreddy S, Kaye KS, Sobel JD. Fluconazole-Resistant Candida albicans Vulvovaginitis: Obstetrics & Gynecology. 2012 Dec;120(6):1407–14. Available from: <URL>.

13. Figueroa-Quintanilla D, Salazar-Lindo E, Sack RB, Leon-Barua R, Sarabia-Arce S, Campos-Sanchez M, et al. A Controlled Trial of Bismuth Subsalicylate in Infants with Acute Watery Diarrheal Disease. N Engl J Med. 1993 Jun 10;328(23):1653–8. Available from: <URL>.

14. Khodashenas B, Ghorbani HR. Synthesis of silver nanoparticles with different shapes. Arabian Journal of Chemistry. 2019 Dec;12(8):1823–38. Available from: <URL>.

15. Yasin S, Liu L, Yao J. Biosynthesis of silver nanoparticles by bamboo leaves extract and their antimicrobial activity. J Fiber Bioeng Inform. 2013;6(6):77–84.

16. Princy KF, Gopinath A. Spectroscopic Investigation on the Catalytic Efficacy of Biofabricated Gold Nanoparticles using Marine Macroalgae. Materials Today: Proceedings. 2019;9:38–45. Available from: <URL>.

17. Lee HJ, Kim JH, Park SS, Hong SS, Lee GD. Degradation kinetics for photocatalytic reaction of methyl orange over Al-doped ZnO nanoparticles. Journal of Industrial and Engineering Chemistry. 2015 May;25:199–206. Available from: <URL>.

18. Goel M, Das A, Ravikumar K, Asthana A. A study on the enhancement of sonochemical degradation of eosin B using other advanced oxidation processes. Desalination and Water Treatment. 2014;52(34–36):6770–6. Available from: <URL>.

19. Peng F, Cai L, Yu H, Wang H, Yang J. Synthesis and characterization of substitutional and interstitial nitrogen-doped titanium dioxides with visible light photocatalytic activity. Journal of Solid State Chemistry. 2008 Jan;181(1):130–6. Available from: <URL>.

20. Tetenbaum M, Hash M, Tani BS, Luo JS, Maroni VA. Oxygen stoichiometry, phase stability, and thermodynamic behavior of the lead-doped Bi-2223 and Ag/Bi-2223 systems. Physica C: Superconductivity. 1995 Jul;249(3–4):396–402. Available from: <URL>.

21. Al-Shamali SS. Photocatalytic degradation of methylene blue in the presence of TiO2 catalyst assisted solar radiation. Australian Journal of Basic and Applied Sciences. 2013;7(4):172–6.

22. Omrani AA, Taghavinia N. Photo-induced growth of silver nanoparticles using UV sensitivity of

cellulose fibers. Applied Surface Science. 2012 Jan;258(7):2373–7. Available from: <URL>.

23. Patil CD, Borase HP, Patil SV, Salunkhe RB, Salunke BK. Larvicidal activity of silver nanoparticles synthesized using Pergularia daemia plant latex against Aedes aegypti and Anopheles stephensi and nontarget fish Poecillia reticulata. Parasitol Res. 2012 Aug;111(2):555–62. Available from: <URL>.

24. Sylvestre JP, Kabashin AV, Sacher E, Meunier M, Luong JHT. Stabilization and Size Control of Gold Nanoparticles during Laser Ablation in Aqueous Cyclodextrins. J Am Chem Soc. 2004 Jun 1;126(23):7176–7. Available from: <URL>.

25. Al-Shamali SS. Photocatalytic degradation of methylene blue in the presence of TiO2 catalyst assisted solar radiation. Australian Journal of Basic and Applied Sciences. 2013;7(4):172–6.

26. Bhuiyan MSH, Miah MY, Paul SC, Aka TD, Saha O, Rahaman MM, et al. Green synthesis of iron oxide nanoparticle using Carica papaya leaf extract: application for photocatalytic degradation of remazol yellow RR dye and antibacterial activity. Heliyon. 2020;6(8). Available from: <URL>.

27. Alem AF, Worku AK, Ayele DW, Wubieneh TA, Teshager AA, Tadele Mihret Kndie, et al. Ag doped Co3O4 nanoparticles for high-performance supercapacitor application. Heliyon. 2023 Feb;9(2):e13286. Available from: <URL>.

28. ElBatal FH, Marzouk MA, ElBatal HA, EzzElDin FM. Impact effect of gamma irradiation on the optical, FTIR, ESR spectral properties and thermal behavior of some mixed (PbO + Bi2O3) borate glasses searching for shielding effects. Journal of Molecular Structure. 2022 Nov;1267:133602. Available from: <URL>.

29. Wahlbeck PG, Myers DL, Salazar KV. Bismuth activities in a lead-doped bismut-2223 superconductor. Physica C: Superconductivity. 1995 Oct;252(1–2):147–54. Available from: <URL>.

30. Lu CH, Chen YC. Characterization of lead cation-incorporated strontium bismuth tantalate ferroelectrics. Integrated Ferroelectrics. 2000;31(1–4):129–38.

31. Koli Prashant B, Kapadnis Kailas H. Green synthesis and characterization of SnO2 and ZnO nanoparticles: Study their electrical conductivity and gas sensing properties. Der ChemicaSinica. 2016;7(2):29–35.

32. Li R, Chen W, Kobayashi H, Ma C. Platinum-nanoparticle-loaded bismuth oxide: an efficient plasmonic photocatalyst active under visible light. Green Chem. 2010;12(2):212. Available from: <URL>.

33. Mohammed-Brahim B, Buchet JP, Lauwerys R. Erythrocyte pyrimidine 5′-nucleotidase activity in workers exposed to lead, mercury or cadmium. International archives of occupational and environmental health. 1985;55:247–52.